IOP Publishing Journal of Physics D: Applied Physics
J. Phys. D: Appl. Phys. **54** (2021) 104003 (7pp) https://doi.org/10.1088/1361-6463/abc84a

Modelling of the magnetization reversal of nanocomposites consisting of core–shell particles

Sergey G Erokhin and Dmitry V Berkov

General Numerics Resear Lab, Moritz-von-Rohr-Str. 1A, Jena 07745, Germany

E-mail: d.berkov@general-numerics-rl.de

Received 10 August 2020, revised 28 October 2020
Accepted for publication 6 November 2020
Published 22 December 2020

Abstract

We performed large-scale micromagnetic simulations on core–shell particle systems for $SrFe_{12}O_{19}/Fe$ and $CoFe_2O_4/Co$ nanocomposites, where both magnetically hard and soft materials were considered as the core or shell materials of these particles. A detailed analysis of the influence of structural properties and exchange core–shell coupling within the same particle on the magnetization reversal of a nanocomposite was carried out, revealing different remagnetization scenarios in terms of the evolution of magnetization distributions in soft magnetic cores. The optimal nanocomposite compounds with respect to the energy product of material were predicted.

Keywords: ferrites, nanocomposites, permanent magnets, micromagnetism, simulation, core–shell structure

(Some figures may appear in colour only in the online journal)

1. Introduction

The key advantage of composite materials is the possibility to tailor their properties for a particular application. In this regard, magnetic nanocomposites (Stamps *et al* 2014, Coey 2012) may be used as an example: combining the so called 'hard' (high-anisotropy) and 'soft' (low-anisotropy) magnetic materials, possessing high coercivity and large magnetization correspondingly, has opened up new pathways in the manufacturing of nanocomposites that are considered as promising candidates for permanent magnet applications.

The main challenge in the development of such materials is the prediction of optimal structural parameters and magnetic coupling in a system comprising of nano-sized elements. One of the most effective approaches is supposed to be the usage of the core–shell morphology of material's grains due to the large area of the interface between the hard and soft phases, allowing for improvement of the magnetic coupling between them (Song and Zhang 2012). The same problem of the core–shell structure optimization is being solved regarding magnetic nanoparticles in various application from very different research areas, e.g. magnetic recording media in computer technology, drug delivery and diagnostic kits in bioengineering and medicine, etc. A comprehensive review devoted to these problems has been published by López-Ortega and coauthors (López-Ortega *et al* 2015), where diverse questions of the manufacturing of bi-magnetic core–shell particles and their perspective applications including permanent magnets, microwave absorption and biomedical technologies are addressed.

Further optimization of magnetic nanocomposites based on core–shell particles requires a thorough understanding of the magnetic structure and its evolution during the magnetization reversal process in these materials. Taking into account the complexity of intra- and interparticle interactions within this system, numerical simulations represent an indispensable tool to achieve this goal. The present paper contains a detailed micromagnetic modeling of core–shell structured nanocomposites based on the example of two sets of magnetic materials: $\{SrFe_{12}O_{19}, Fe\}$ and $\{CoFe_2O_4, Co\}$. This choice has been motivated by the wider availability of ferrites as raw materials, their low cost and corrosion resistance in contrast to their rare-earth counterparts. Additionally, there have been a large number of successful attempts manufacturing

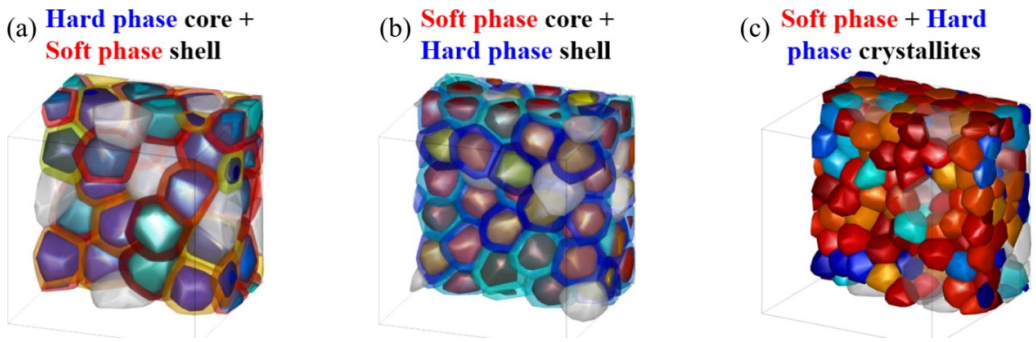

Figure 1. Examples of generated structures (cold colors correspond to the hard phase, warm colors to the soft phase, transparent polyhedrons—to pores). (a) Hard phase core and soft phase shell sample, (b) soft phase core and hard phase shell sample, (c) sample composed of individual hard and soft phase crystallites.

core–shell particles, where either monometallic (i.e. consisting of only one metal) particles with a significant magnetization a require protective anti-oxidation layer (magnetic or nonmagnetic), or different ferrites may play the role of core or shell. From the 'manufacturing' point of view, magnetic nanoparticles obtained by thermal decomposition may consist of various combinations of hard/soft magnetic materials, such as $Fe/CoFe_2O_4$ (Yoon *et al* 2011), $CoFe_2O_4/ZnFe_2O_4$ (Masala *et al* 2006) and $CoFe_2O_4/MnFe_2O_4$ (Lee *et al* 2011, Song and Zhang 2012). By using other process types—co-precipitation (Zhang and Li 2009) and chemical reduction (Soares *et al* 2013)—the compositions $SrFe_{12}O_{19}/CoFe_2O_4$ and $CoFe_2O_4/CoFe_2$ can be produced correspondingly.

In this work, the influence of the structural and magnetic parameters of core–shell nanocomposites on their coercivity, remanence and maximal energy product are studied. The obtained results are compared with corresponding results for nanocomposites composed of individual monomaterial grains of different (hard and soft) phases. Details of the magnetization distribution in soft magnetic cores are revealed.

2. Simulation methodology

We have developed a methodology for the simulation of magnetization reversal in systems of core–shell particles (figure 1), which also may contain pores; in all following simulations the volume fraction of pores is 20%. This methodology is based on our novel approach of modeling magnetic nanocrystalline materials, which employs a special polyhedron discretization of a simulated sample and was very successfully applied to several fundamentally interesting and application-relevant systems (see, e.g. Erokhin *et al* 2012, Erokhin *et al* 2018). As usual, we take into account all four standard contributions to the total magnetic free energy: energy in the external field, magnetocrystalline anisotropy energy, exchange stiffness and magnetodipolar interaction energies. The main advantage of our method is the combination of the flexible description of a nanocomposite structure—as in general finite element schemes—with the possibility to use Fast Fourier Transformation for the rapid calculation of the long-ranged magnetodipolar interaction field; further details can be found in (Michels *et al* 2014, Erokhin and Berkov 2017).

In our simulation of core–shell particles, special attention has been paid to the shape of the crystallite cores: as can be seen in figure 1, this shape resembles the shape of the corresponding crystallite resulting in the almost constant thickness of the grain's shell, which conforms to its physical realization during the manufacturing process. This feature was implemented using the procedure that scales down the crystallite's shape and forms the core by meshing elements inside this new shape.

In our simulations, we have used the system volume $230 \times 230 \times 230\,\mathrm{nm}^3$, discretized in $\approx 2 \times 10^5$ finite elements with the typical size 4 nm, so that we could calculate the magnetization reversal for samples of 600… 30 particles (depending on the average particle size varying in the range of 24–62 nm correspondingly). Periodic boundary conditions are used in all presented simulations. The employed discretization allows us to resolve the magnetization distribution in both phases with up to 6000 mesh elements per particle. Additionally, for every set of parameters, the results have been obtained and averaged over four different geometrical realizations. Finally, the magnetic performance of the core–shell structured nanocomposites was compared with systems composed of individual hard and soft crystallites (see figure 1(c)) with corresponding concentrations of hard and soft phases and the same sizes of soft magnetic grains.

The magnetic parameters of materials used in our modeling correspond to their standard values (see, e.g. Coey 2010, chapter 11.6) and are summarized in table 1, where M_s is the saturation magnetization, K—the anisotropy constant and A—the exchange stiffness constant. For both pairs, i.e. $\{SrFe_{12}O_{19}, Fe\}$ and $\{CoFe_2O_4, Co\}$ we have studied both situations: a hard magnetic core surrounded by a soft magnetic shell and a soft core covered by a hard shell. The notation $SrFe_{12}O_{19}/Fe$ means that grains of the nanocomposite consists of Sr-ferrite cores and iron shells; $Fe/SrFe_{12}O_{19}$ indicates the opposite situation.

The anisotropy axes of the hard phase (cores or shells) in all simulation sets are directed along the applied magnetic field. This choice was motivated as the simplest possible one to achieve the maximal performance of a nanocomposite intended as permanent magnet material. The variation of the

Table 1. Magnetic parameters used in the modeling of core–shell structured nanocomposites.

	$SrFe_{12}O_{19}$	Fe	$CoFe_2O_4$	Co
M_s(G)	400	1700	450	1400
Anisotropy type	Uniaxial	Cubic	Cubic	Cubic
K (erg cm^{-3})	4.0×10^6	5.0×10^5	3.0×10^6	6.0×10^5
A (erg cm^{-1})	0.6×10^{-6}	2.0×10^{-6}	0.7×10^{-6}	3.0×10^{-6}

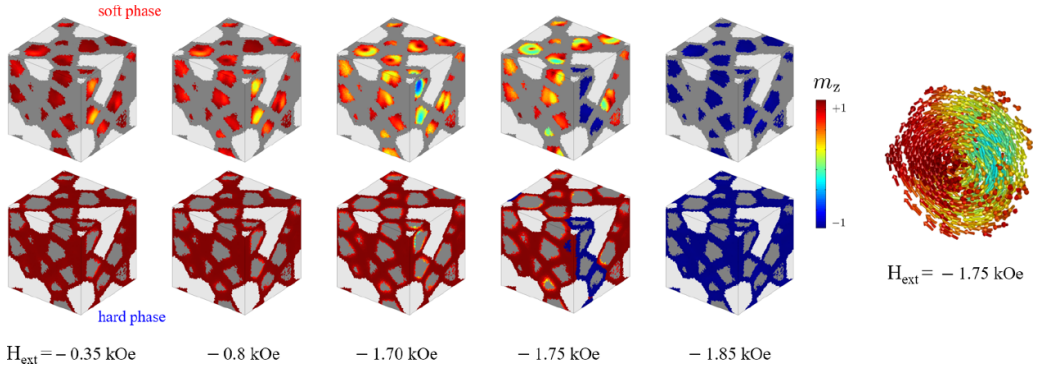

Figure 2. Evolution of the magnetization distribution during the remagnetization process in the $Fe/SrFe_{12}O_{19}$ structure ($d_{core} = 50$ nm, $d_{shell} = 12$ nm, $\kappa_{ext} = 0, \kappa_{int} = 1$). The upper row shows the soft phase (cores), the lower row—the hard phase (shells); the light grey areas in both rows are pores. The magnetic vortex-like structure in an individual core is presented in the right panel.

anisotropy direction inside core and/or shell can be included in our model at the later stages, when the optimal manufacturing process for such particles will be established.

Exchange coupling in our methodology is governed by the parameter κ: the exchange energy between two mesh elements is multiplied by κ, if they belong to different grains or to core and shell of the same grain. Therefore $\kappa = 0$ denotes the situation of exchange decoupled mesh elements, while $\kappa = 1$ corresponds to the full coupling. Weakening of the coupling between the core and the shell of the same grain (internal coupling) is denoted below by κ_{int}, coupling between the shells of different grains (external coupling)—by κ_{ext}.

3. Results and discussion

3.1. $Fe/SrFe_{12}O_{19}$ *composites*

We begin with the analysis of the magnetization reversal process in the composite consisting of $Fe/SrFe_{12}O_{19}$ core–shell particles. An example of the evolution of the magnetization distribution in such a sample consisting of large particles ($d_{core} = 50$ nm, $d_{shell} = 12$ nm) is presented in figure 2, where those distributions are shown for cores and shells separately for better visualization. In this example, the exchange coupling between different crystallites—coupling between shells in this case—is absent ($\kappa_{ext} = 0$), but the core and shell of every individual crystallite are perfectly coupled: $\kappa_{int} = 1$. As can be clearly seen, the main feature of the remagnetization process is the formation of 3D vortex or vortex-like structures in the soft magnetic cores, while hard ferrite shells remain in a single-domain state despite strong coupling with the corresponding core. Up to $H_{ext} = -1.70$ kOe the whole hard phase is still magnetized along the initial applied magnetic field (z-direction), but magnetic moments of the soft iron cores started to deviate from this direction already in small positive fields due to the internal demagnetizing field. At $H_{ext} = -1.75$ kOe some cores have completely reversed their magnetization, 'dragging' their shells primarily by the intergrain exchange interaction. This effect leads to the coercive field of $H_c \approx 1.8$ kOe for this system with the completion of the remagnetization at $H_{ext} = -1.85$ kOe.

The influence of the exchange coupling between core and shell on the remagnetization process in a nanocomposite for $Fe/SrFe_{12}O_{19}$ with $d_{core} = 30$ nm and $d_{shell} = 8$ nm is demonstrated in figure 3. The interparticle exchange coupling is absent as in the previous example, while the coupling between cores and shells of the same grain (κ_{int}) is varied in the whole range $\kappa_{int} = 0 \ldots 1$. The dependence of the total hysteresis loop and the corresponding normalized partial (i.e. for core or shell only) hysteresis curves on κ_{int} indicate the transformation from the two-phase behaviour—where the magnetization reversal of shells is decoupled from the reversal of cores—to the simultaneous reversal of both phases in an exchange coupled system. Analyzing the remagnetization of the constituent phases (red and blue dotted curves), we conclude that the coupling strength $\kappa_{int} = 0.2$ is almost sufficient to force both phases to remagnetize simultaneously. Further increase of κ_{int} to 0.5 results in achieving the maximal (for this parameter set) coercive field of about 3 kOe without an additional improvement from the coupling enlargement.

The 'average' magnetization state of particles (and also for cores and shells separately) at various remagnetization stages can be effectively represented by introducing an average total magnetization $|M|$ of cores or shells as a function of the external field. If $|M_i| = \sqrt{(M_{x,i}^2 + M_{y,i}^2 + M_{z,i}^2)}$ is the absolute value of the magnetization of, for example the i-core, then

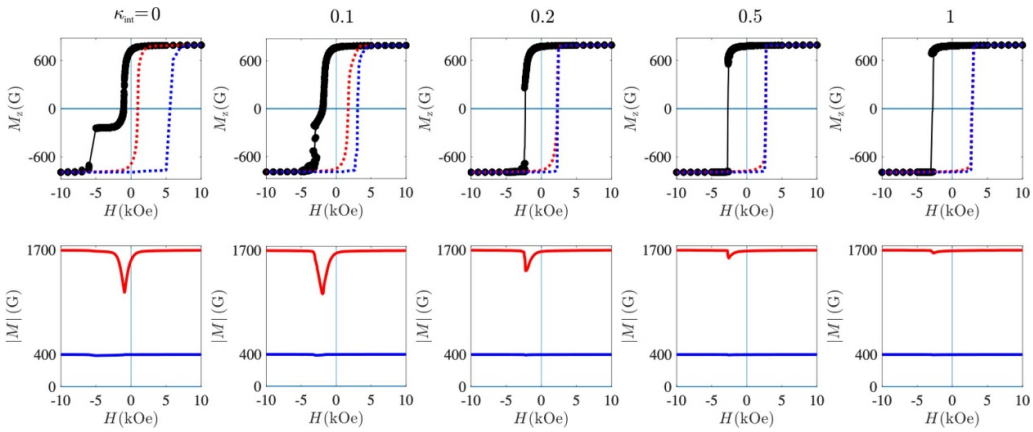

Figure 3. Hysteresis curves and $|M(H)|$ dependencies for different exchange couplings κ_{int} between core and shell in the system $Fe/SrFe_{12}O_{19}$ (soft phase cores and hard phase shells) with $d_{\text{core}} = 30\,\text{nm}$, $d_{\text{shell}} = 8\,\text{nm}$, $\kappa_{\text{ext}} = 0$. Connected black dots show upper parts of the total hysteresis curves, red and blue dotted lines—lower parts of normalized hysteresis loops for soft and hard phases correspondingly. The same color coding applies to solid lines in $|M(H)|$ dependencies in the lower row, indicating the strong deviation of soft phase cores from the single-domain state in the systems with the weak exchange coupling.

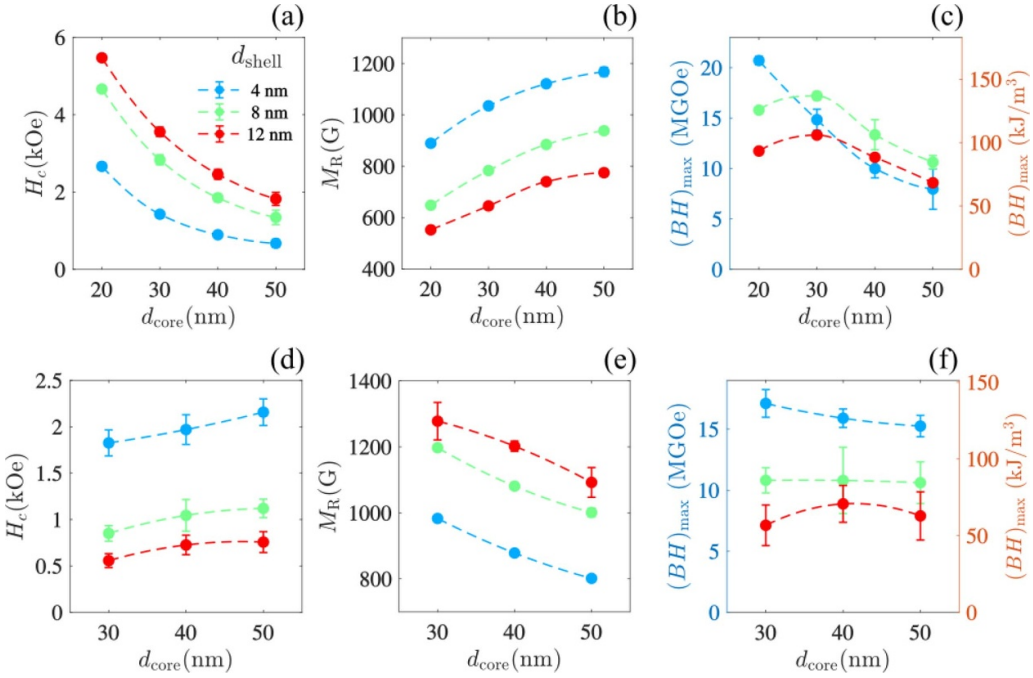

Figure 4. Coercive field, remanence and energy product of the system $\{SrFe_{12}O_{19}, Fe\}$ in the case of soft phase core and hard phase shell (a)–(c) and hard phase core and soft phase shell (d)–(f) as functions of the core diameter for various shell thicknesses ($\kappa_{\text{ext}} = 0, \kappa_{\text{int}} = 1$).

averaging over all cores gives $|M|$, which can serve as a good measure for the deviation of the core's magnetization state from the single-domain state, corresponding to $|M| = M_s$. Plotting this quantity for different phases, as distinctly demonstrated in figure 3 (lower row), we can see that the hard phase shells are always in a single-domain state, while soft cores strongly deviate from this state in the systems with a weak exchange coupling.

The preservation of the almost perfect single-domain state of soft magnetic cores by their full exchange coupling with shells ($\kappa_{\text{int}} = 1$) radically distinguishes this system ($d_{\text{core}} = 30\,\text{nm}$) from the analogous one from the previous example with the much larger core diameter ($d_{\text{core}} = 50\,\text{nm}$), where the formation of the core vortex is a characteristic feature. The single-domain state of 30 nm-cores leads to the coercivity to 3.0 kOe; as the remanence in both systems is nearly the same, it results in the 2.5 ×-gain of the energy product.

A summary of simulation results for the nanocomposite $Fe/SrFe_{12}O_{19}$ is given in the upper row of figure 4. As demonstrated above, a particle core made of a soft material exhibits significant deviations from the single-domain state starting from some critical diameter $d_{\text{core}}^{\text{cr}}$. The results for this case are summarized in the upper row of figure 4. It can be seen that when increasing the soft core diameter for the given hard shell thickness, the system coercivity strongly decreases due to the increase of the fraction of the soft magnetic material,

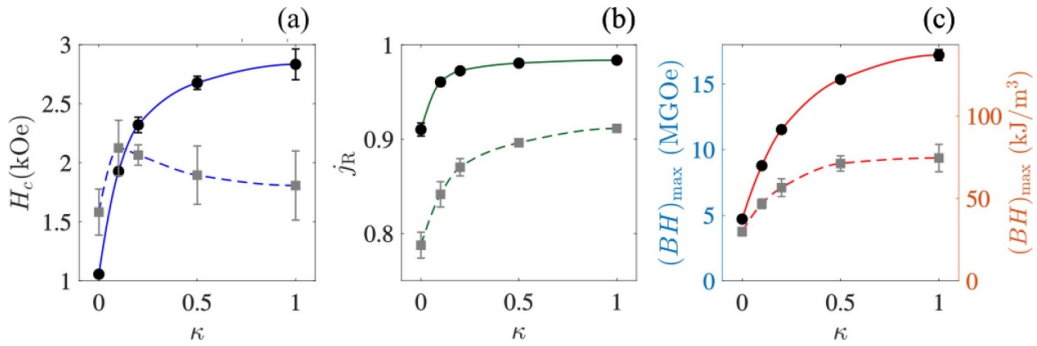

Figure 5. Coercive field (a), normalized remanence (b) and energy product (c) of the system $Fe/SrFe_{12}O_{19}$ in the case of the soft phase core and hard phase shell (solid lines) and of the system composed of single-phase hard and soft crystallites (dashed lines) with the same phase volume fractions, presented as functions of the exchange weakening κ. For the core–shell system $\kappa_{int} = \kappa$ and $\kappa_{ext} = 0$.

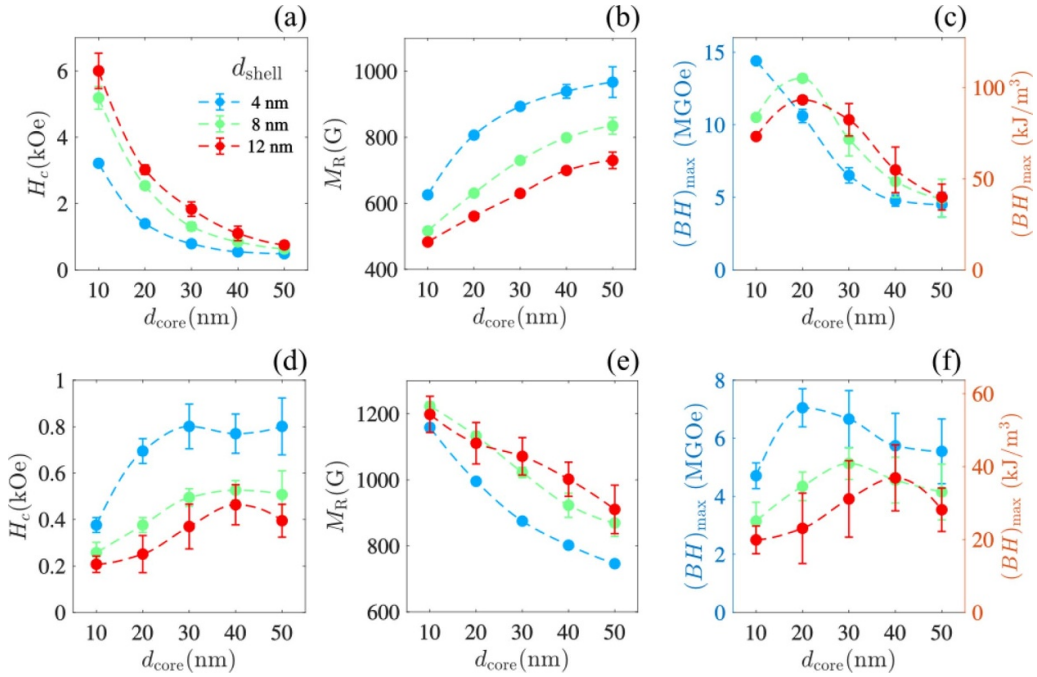

Figure 6. Coercive field, remanence and energy product of the system $\{CoFe_2O_4, Co\}$ in the cases of soft phase core and hard phase shell (a)– (c) and of hard phase core and soft phase shell (d)–(f), plotted as functions of the core diameter for various shell thicknesses.

because it has a lower anisotropy. The same increase of the soft phase fraction is responsible for the significant remanence enhancement, because the soft material has a larger magnetization. These two concurrent trends lead to the overall decrease of the energy product as the function of the d_{core}, because the coercivity decreases more than the remanence increases.

Analogous simulations have been performed also for the opposite case—$SrFe_{12}O_{19}/Fe$ system, i.e. grains consisting of a hard magnetic core and soft magnetic shell. Cumulative results for this system are collected in the lower row of figure 4. Inspection of magnetization distributions in both phases (not shown) has revealed that even for the largest shell thickness each soft shell remains approximately single-domain during the magnetization reversal process, and cores remain in an almost perfect single-domain state. As a result, with increasing core diameter for the given soft shell thickness the coercivity of the nanocomposite slightly increases, whereby the remanence correspondingly decreases; analogously to the explanation for the previous case, both features are due to the increasing volume factor of the hard phase which has the larger anisotropy and lower saturation magnetization. Due to these opposite trends, the energy product as a function of the core diameter remains in this case approximately the same (figure 4(f)).

In terms of this product, both systems analyzed in figure 4 provide a comparable and very high performance.

The efficiency of the core–shell approach for manufacturing the high-performance materials for various applications can be demonstrated by the comparison of the main parameters of their hysteresis loops (coercivity, remanence and energy product) with corresponding results of the system composed of individual hard and soft crystallites. An example of such a structure is presented in figure 1(c). These systems were generated with the same volume fractions of soft and hard phases

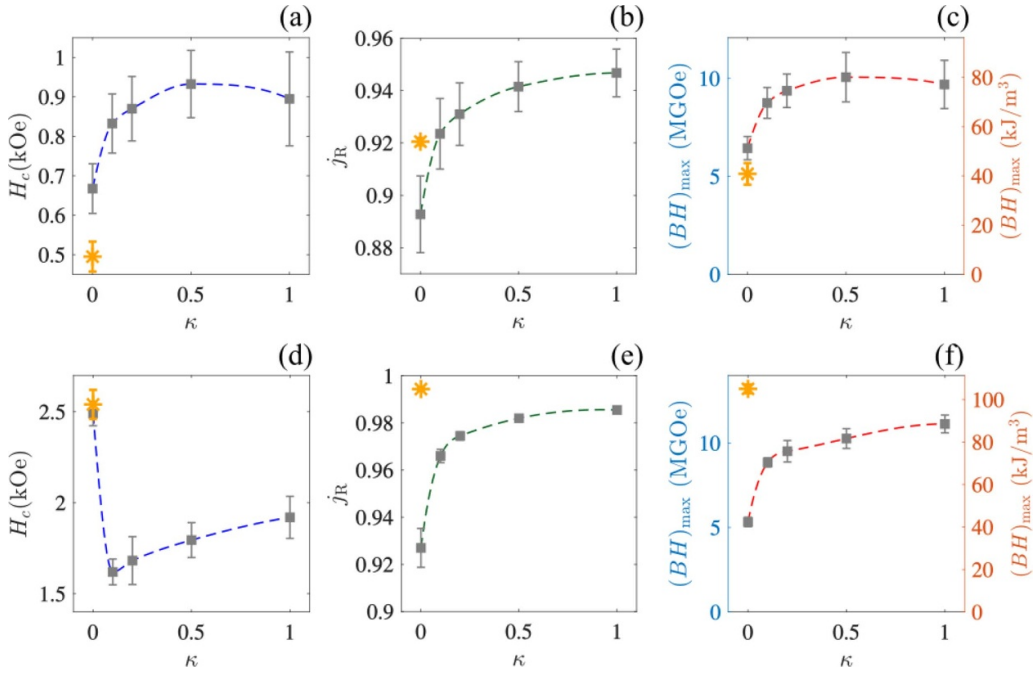

Figure 7. From left to right: coercive field, normalized remanence and energy product of the core–shell system (dark yellow asterisks) and of the system composed of single-phase hard and soft crystallites (dashed lines) with corresponding volume fractions as functions of the exchange weakening κ (for the core–shell system $\kappa_{int} = \kappa$ and $\kappa_{ext} = 0$. Upper row (a)–(c): $CoFe_2O_4/Co$ system (core–shell grains have $d_{core} = 30$ nm and $d_{shell} = 8$ nm), lower row (d)–(f): $Co/CoFe_2O_4$ system (core–shell grains have $d_{core} = 20$ nm and $d_{shell} = 8$ nm).

as their core–shell counterparts including 20% porosity. In addition, the volume of individual crystallites was chosen to be approximately equal to the volume of cores in the core–shell-particle composites. In the case of individual single-phased crystallites (grain), the exchange weakening on the intergrain boundary is governed by only one parameter κ, which is the same for boundary between crystallites of the same phase and of different phases.

Comparison of simulated properties for the core–shell nanocomposite $Fe/SrFe_{12}O_{19}$ ($d_{core} = 30$ nm, $d_{shell} = 8$ nm and $\kappa_{ext} = 0$) to the equivalent single-phase-particles composite (volume fractions are 56% and 24% for soft and hard phases correspondingly) is presented in figure 5; note that for core–shell structures $\kappa_{int} = \kappa$ and $\kappa_{ext} = 0$. This composition was chosen for the comparison for two reasons: first, it corresponds to the local maximum of the energy product (see figure 4(c)) and second, this system has a comparatively large core, for which the magnetization might demonstrate different reversal scenarios depending on the exchange coupling with the shell—from a vortex-like structure at $\kappa_{int} = 0$ to the almost single-domain state at $\kappa_{int} = 1$ (figure 3).

The results presented in figure 5, demonstrate that while both systems are comparable (in terms of their energy product) for the weak exchange coupling, the core–shell system strongly outperforms its counterpart consisting of single-phase-particles, when the exchange coupling becomes larger. Already for $\kappa > 0.1$ the effect of the larger interface area between hard and soft phases in the core–shell grain structure starts to play a decisive role in its better performance compared to the system composed of individual single-phase particles. Thus, when reaching $\kappa = 0.5$, with a much higher coercivity and an almost maximal remanence, the core–shell structured nanocomposite achieves a two times larger energy product.

3.2. $Co/CoFe_2O_4$ *composites*

The system containing $CoFe_2O_4$ and Co has been studied using the broader range of parameters (see figure 6) for both core/shell material choices. One of the most important results of this modeling is the observation that even for the largest shell thickness the soft shell remains approximately single-domain due to the larger exchange coupling and smaller magnetization of Co in comparison to Fe (see table 1). As in the previous case of the $\{SrFe_{12}O_{19}, Fe\}$-pair, the hard phase is in an almost perfect single-domain state during the remagnetization process for the all parameter sets.

In the system of particles having the soft phase core and hard phase shell (figure 6, upper row), for the given shell thickness the coercivity strongly decreases with the core diameter, while the remanence increases, although not as strongly as the coercivity decreases; the reasons for these trends are the same as discussed for the previous pair of magnetic materials. The resulting energy product dependence on the core diameter is non-monotonic for two largest shell thicknesses, and decreases for all studied d_{shell} for $d_{core} > 20$ nm. As for the previous system, this set of parameters for both core and shell are in an almost perfect single-domain state. For these materials, the soft phase shell and hard phase core system is clearly superior in terms of the energy product, which can be as large as 14 MG · Oe.

In the opposite case of a (hard phase core)/(soft phase shell)-system (lower row at figure 6), coercivity slightly

increases and the remanence correspondingly decreases with increasing the core diameter (for the given shell thickness), which is also due to the decrease of the volume fraction of the soft phase. For the given shell thickness, there always exists an optimal core diameter (which provides the maximal energy product) due to the specific character of opposite trends for coercivity and remanence as functions of d_{core}.

The similar comparison with the nanocomposite consisting of single-phase grains as for the $Fe/SrFe_{12}O_{19}$-pair has been made for two compositions: (i) $CoFe_2O_4/Co$ with $d_{\text{core}} = 30\,\text{nm}$, $d_{\text{shell}} = 8\,\text{nm}$ and (ii) $Co/CoFe_2O_4$ with $d_{\text{core}} = 20\,\text{nm}$, $d_{\text{shell}} = 8\,\text{nm}$. The first set of parameters was chosen as a representative of the average result obtained for this nanocomposite type (see figure 6, lower row). If this result is compared with the coercivity, remanence and energy product of a nanocomposite with the same phases volume fraction, but composed of single-phased grains (figure 7, upper row), it becomes clear that such an *unoptimized* composition of core–shell particles is unable to compete with a 'standard' nanocomposite. The situation is the opposite in the case of the soft core and hard shell composition with the optimized parameters (figure 6, upper row). The local maximum at $d_{\text{core}} = 20\,\text{nm}$ in terms of the energy product results in the strong advantage of the core–shell scheme against the system composed of single-phase grains (figure 7, lower row). We note that this advantage is observed for all values of exchange coupling parameter κ.

4. Conclusions

We have developed and tested a micromagnetic methodology for modelling the magnetization reversal of nanocomposites consisting of core–shell-structured grains (particles). This approach enables us to simulate systems consisting of a large number of grains, thus obtaining results with a high statistical accuracy and allowing us to provide recommendations for the optimization of magnetic materials based on the core–shell particles before their actual manufacturing. Using our methodology, we have demonstrated that both main parameters of the material hysteresis (coercivity and remanence) strongly depend on the core diameter and the shell thickness of the constituting core–shell particles. Complicated interplay of opposite trends in the dependence of coercivity and remanence on these particle parameters can result in different corresponding dependencies of the most important material characteristic—its energy product. Our simulations show, that for the optimal structural parameters, the energy product of nanocomposites consisting of defect-free core–shell particles based on monometallic (iron) and ferrite materials can achieve approximately 15 MG · Oe, which is significantly larger than for corresponding materials made of single-phase nanoparticles. The comparison of the core–shell nanocomposite with its equivalent composed of individual hard and soft crystallites demonstrates the advantage of the core–shell approach, with up to 2 times the energy product due to the enlarged area of the interface between phases.

Acknowledgment

Authors gratefully acknowledge financial support of EU-H2020 AMPHIBIAN Project (720853).

ORCID iDs

Sergey G Erokhin https://orcid.org/0000-0001-8449-3612
Dmitry V Berkov https://orcid.org/0000-0003-3883-5161

References

Coey J M D 2010 *Magnetism and Magnetic Materials* (Cambridge: Cambridge University Press)
Coey J 2012 Permanent magnets: plugging the gap *Scr. Mater.* **67** 524–9 (Viewpoint Set No. 51: Magnetic Materials for Energy)
Erokhin S and Berkov D 2017 Optimization of nanocomposite materials for permanent magnets: micromagnetic simulations of the effects of intergrain exchange and the shapes of hard grains *Phys. Rev. Appl.* **7** 014011
Erokhin S, Berkov D, Gorn N and Michels A 2012 Micromagnetic modeling and small-angle neutron scattering characterization of magnetic nanocomposites *Phys. Rev.* B **85** 024410
Erokhin S, Berkov D, Ito M, Kato A, Yano M and Michels A 2018 Towards understanding of magnetization reversal in Nd–Fe–B nanocomposites: analysis by high-throughput micromagnetic simulations *J. Phys.: Condens. Matter.* **30** 125802
Lee J-H *et al* 2011 Exchange-coupled magnetic nanoparticles for efficient heat induction *Nat. Nanotechnol.* **6** 418–22
López-Ortega A, Estrader M, Salazar-Alvarez G, Roca A G and Nogués J 2015 Applications of exchange coupled bi-magnetic hard/soft and soft/hard magnetic core/shell nanoparticles *Phys. Rep.* **553** 1–32
Masala O, Hoffman D, Sundaram N, Page K, Proffen T, Lawes G and Seshadri R 2006 Preparation of magnetic spinel ferrite core/shell nanoparticles: soft ferrites on hard ferrites and vice versa *Solid State Sci.* **8** 1015–22
Michels A, Erokhin S, Berkov D and Gorn N 2014 Micromagnetic simulation of magnetic small-angle neutron scattering from two-phase nanocomposites *J. Magn. Magn. Mater.* **350** 55–68
Soares J, Galdino V, Conceição O, Morales M, de Araújo J and Machado F 2013 Critical dimension for magnetic exchange-spring coupled core/shell CoFe2O4/CoFe2 nanoparticles *J. Magn. Magn. Mater.* **326** 81–4
Song Q and Zhang Z J 2012 Controlled synthesis and magnetic properties of bimagnetic spinel ferrite CoFe2O4 and MnFe2O4 nanocrystals with core–shell architecture *J. Am. Chem. Soc.* **134** 10182–90
Stamps R L *et al* 2014 The 2014 magnetism roadmap *J. Phys. D: Appl. Phys.* **47** 333001
Yoon T-J, Lee H, Shao H and Weissleder R 2011 Highly magnetic core–shell nanoparticles with a unique magnetization mechanism *Angew. Chem., Int. Ed.* **50** 4663–6
Zhang L and Li Z 2009 Synthesis and characterization of SrFe12O19/CoFe2O4 nanocomposites with core-shell structure *J. Alloys Compd.* **469** 422–6